Available online at www.sciencedirect.com

SciVerse ScienceDirect

Ceramics International 39 (2013) 323–330

CERAMICS INTERNATIONAL

www.elsevier.com/locate/ceramint

Effect of organic capping agent on the photocatalytic activity of MgO nanoflakes obtained by thermal decomposition route

R. Sathyamoorthy[a,*], K. Mageshwari[a], Sawanta S. Mali[b], S. Priyadharshini[a], Pramod S. Patil[b]

[a]PG and Research Department of Physics, Kongunadu Arts and Science College, Coimbatore 641029, Tamilnadu, India
[b]Thin Film Materials Laboratory, Department of Physics, Shivaji University, Kolhapur 416004, India

Received 17 April 2012; received in revised form 7 June 2012; accepted 8 June 2012
Available online 16 June 2012

Abstract

In the present work we report a facile and eco-friendly route to synthesize magnesium oxide (MgO) nanoflakes by thermal decomposition of precursors, which are prepared by a reflux condensation approach using different solvents namely ethylenediamine (EDA), hexamethylediamine (HTMA) and triethanolamine (TEA). X-ray diffraction (XRD) pattern reveales the polycrystalline nature of MgO with cubic structure. Fourier transform infrared spectroscopy (FTIR) studies confirmed the formation of MgO with the characteristic vibrational mode of Mg–O. Scanning electron microscopy (SEM) images revealed the formation of MgO nanoflakes. Optical band gap energy of MgO nanocrystals calculated from UV diffused reflectance spectroscopy (DRS) varied from 5.42 to 5.56 eV. Photoluminescence (PL) spectra exhibited visible emissions due to the formation of defects in the band gap region of MgO. The photocatalytic degradation of methyl orange (MO) dye by MgO nanoflakes synthesized using different solvents was investigated under UV light irradiation and the results demonstrate that MgO nanoflakes possess appreciable photocatalytic activity for decomposing MO dye, when EDA is used as a capping agent.

Keywords: A. Powders: chemical preparation; B. Defects; B.Grain size; C. Optical properties

1. Introduction

In recent years, considerable attention has been paid globally to eradicate the hazardous materials from wastewater. The wastewater from pulp and paper industry contains huge amounts of organic matter with high chemical stability, low biodegradability, high color, high adsorbable organic halogenated compounds (AOX) and toxicity values, which are potentially harmful to the eco-environment [1,2]. The traditional methods employed to reduce the above mentioned parameters do not destroy these compounds, hence futile in completely removing the toxic organic compounds, and merely transfer dyes from the liquid to solid phase causing secondary pollution, and thus requiring further treatment [3]. Advanced oxidation processes (AOPs) using metal oxide semiconductor mediated nano-photocatalysis have emerged as an alternative technique for the total oxidation of hazardous organic compounds. The efficiency of these systems is based on the production of reactive oxygen species (ROS) such as superoxides and hydroxyl radicals which are able to oxidize almost all organic pollutants to carbon dioxide, water and mineral acids [4,5]. The high surface to volume ratio, large numbers of reactive defect sites, acid and base sites, and surface hydroxyl groups of nano-photocatalysts facilitate enhanced adsorption of the organic compounds leading to high photocatalysis conversion [6]. Over the years, a large number of semiconductor oxides namely TiO_2, ZnO, WO_3, Fe_2O_3 etc., were used as dynamic photocatalyst materials for environmental remediation, especially degradation of organic pollutants in water and air [7–11]. MgO with fascinating properties like very large band gap, excellent thermodynamical stability, low dielectric constant and low refractive index finds extensive applications in catalysis, ceramics, toxic waste remediation,

*Corresponding author: Tel.: +91 422 2642095; fax: +91 422 2644452.
E-mail address: rsathya59@gmail.com (R. Sathyamoorthy).

0272-8842/$36.00
http://dx.doi.org/10.1016/j.ceramint.2012.06.028

and antibacterial materials or as an additive in refractory, paint and superconductor products [12–16]. To date, photocatalytic activity of MgO has been little investigated [17,18]. From the economical and exotoxicological point of view it is noteworthy to investigate the feasibility of using MgO as a dynamic photocatalyst material for degrading the organic pollutants. Accordingly, in the present work we demonstrate the photocatalytic activity of MgO nanoflakes by monitoring the photodegradation of MO dye under UV irradiation. The structural, morphological, optical and photocatalytic activities of synthesized MgO nanoparticles were investigated in detail.

2. Experimental details

2.1. MgO nanocrystals synthesis

All the starting materials were of analytical grade and used without further purification. In a typical synthesis, 0.1 M of magnesium sulfate ($MgSO_4.7\ H_2O$) was prepared in 100 ml of deionized water to form a suspension. To the above suspension, 15 ml of ammonium hydroxide (NH_4OH) solution was injected vigorously under constant stirring at 100 °C, and the mixture was refluxed for 12 h at the same temperature. After the reaction was complete, the solution was cooled naturally to room temperature, and the resulting white precipitate was filtered, washed with deionized water several times to remove the by-products, and finally dried in air at 100 °C for 1 h. The as-synthesized nanocrystals were calcinated at 400 °C for 2 h in air to obtain MgO nanocrystals. To investigate the effect of organic capping agents, $MgSO_4.7\ H_2O$ was mixed with 0.1 M of EDA/TEA/HMTA solution and the reaction was carried out as mentioned above under the same conditions. Herein, the MgO nanocrystals obtained without adding any solvent is designated as sample A, while those obtained by adding HMTA, TEA and EDA were designated as samples B, C, and D respectively.

2.2. Characterization

The structural properties of the MgO nanocrystals were analyzed by XRD using a Bruker AXS D8 advanced X-ray powder diffractrometer equipped with Cu Kα radiation ($\lambda = 0.1541$ nm). FTIR spectrum were recorded on a Bio-Rad (Hercules, CA) FTS-165 spectrometer in the wavelength range 450–4000 cm^{-1}. Surface morphology of the nanocrystals was examined by JEOL JSM-6390LV SEM. The optical band gap of the nanocrystals was estimated from UV DRS using a JASCO V-670 double beam spectrophotometer in the wavelength range 200–300 nm. The photoluminescence (PL) spectrum was recorded using a JOBIN YVON FLUROLOG-3-11 spectroflurometer. The samples were dispersed in ethanol and the measurements were carried out using a Xe lamp with excitation wavelength of 325 nm. High performance liquid chromatography (HPLC, cyber lab) was performed with a binary pump, 1100 UV–vis diode array detector, an autosampler, and a column thermostat. The HPLC system was equipped with a Zorbax C_{18} column (150 × 4.6 mm). The solvent used as a mobile phase was acetonitrile:water (40:60 vol/vol). The flow rate was 0.6 mL min^{-1}, and 20 μL of standard or sample solution was injected.

2.3. Photocatalytic activity

The photocatalytic activity of MgO nanocrystals was evaluated by monitoring the photodegradation of MO dye under stimulated UV irradiation at room temperature. For a typical photocatalytic experiment, 0.2 g of photocatalyst was added to 100 ml of MO aqueous solution (1 mM) with an initial concentration of 10 mg/L. Prior to irradiation, the suspension containing MgO nanopowder and MO dye solution was stirred in the dark for 30 min to achieve adsorption/desorption equilibrium. Then the suspension was irradiated with 5 mW/cm^2 UV light, which was placed 35 cm above the surface of the suspension. During the process of photodegradation, 10 ml of the suspension was tested every 30 min, and centrifuged to separate the photocatalyst particles. Then, the quantitative determination of photocatalytic degradation of MO dye was performed by measuring the characteristic absorption of MO using a UV–vis spectrophotometer (Shimadzu UV1800, $\lambda = 190 - 1100$ nm) at 465 nm [19,20].

The degradation efficiency of MgO was calculated using [21]

$$\text{degradation efficiency } (\%) = \frac{C_O - C}{C_O} \times 100\% = \frac{A_O - A}{A_O} \times 100\% \quad (1)$$

where 'C_O' and 'A_O' represent the initial concentration and absorption of MO solution before irradiation respectively, and 'C' and 'A' are the concentration and absorption of MO solution after irradiation in selected time interval, 't'. The degradation rate constant was calculated from the experimental data using [22]

$$ln\ \frac{C_O}{C} = K_r\ t \quad (2)$$

'K_r' is the degradation rate constant, and 't' is the degradation time. The value of degradation rate constant 'K_r' was obtained from the slope of the kinetics plot.

3. Result and discussion

3.1. Structural analysis

Fig. 1 shows the XRD pattern of MgO nanocrystals prepared using different solvents. All the diffraction peaks in the XRD pattern could be indexed to the polycrystalline MgO with cubic structure, which are consistent with the standard JCPDS card (No. 78-0430). It can be observed that irrespective of the solvent, all the diffraction peaks were considerably broad, indicating formation of small size crystallites. The mean crystallite size (D) of MgO

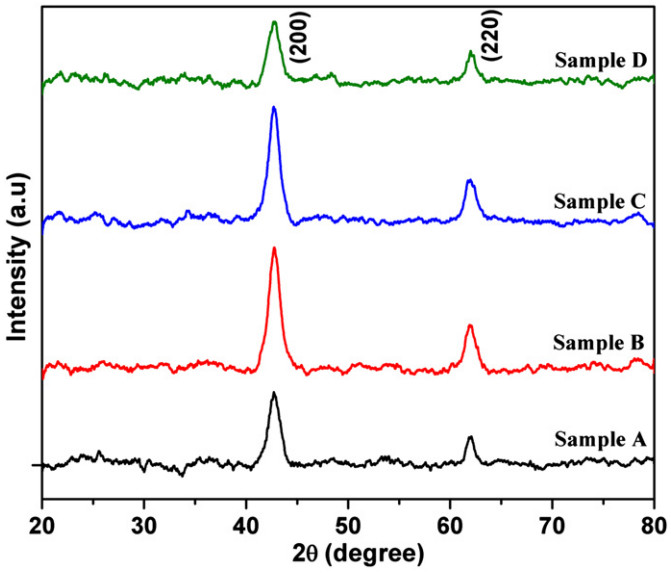

Fig. 1. XRD pattern of MgO nanoflakes prepared using different solvents.

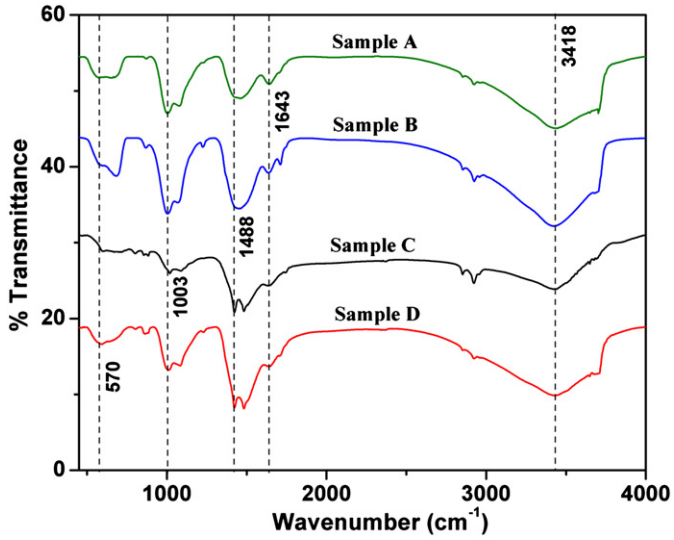

Fig. 2. FTIR spectrum of MgO nanoflakes prepared using different solvents.

Table 1
Structural and optical parameters of MgO nanocrystals prepared using different solvents.

Sample code	Crystallite size D (nm)	Lattice constant a (Å)	Band gap (eV)
A	6	4.239	5.51
B	11	4.229	5.42
C	8	4.222	5.48
D	5	4.234	5.56

nanocrystals was calculated for (200) and (220) planes using the Debye–Scherrer's formula given by Eq. (3), [23]

$$D = \frac{k\lambda}{\beta \ Cos \ \theta} \tag{3}$$

where the constant 'k' is the shape factor $=0.90$, 'λ' the wavelength of X-rays, 'θ' is Bragg's angle, and 'β' is the full width at half maximum. The structural parameters like mean crystallite size, and the lattice constant of MgO nanocrystals calculated from the XRD pattern are given in Table 1.

Fig. 2 shows the FTIR spectrum of MgO nanocrystals prepared using different solvents. It is well known that MgO chemisorbs H_2O and CO_2 molecules from the atmosphere due to its surface acid–base properties [24]. The broad band between 450 and 600 cm^{-1} is associated with the stretching vibrations of MgO [25]. The absorption band around 1003 cm^{-1} possibly arises due to H^- ions [24]. The two absorption peaks at 1643 cm^{-1} and 3418 cm^{-1} are associated with the stretching and bending vibrations, respectively of water [24–26]. The band at 1488 cm^{-1} is attributed to carbonate ions on the surface of the sample, due to adsorption from atmospheric carbon dioxide [25,27].

3.2. Morphological analysis

Fig. 3 shows the SEM image of MgO nanocrystals. SEM images of MgO nanocrystals synthesized using different solvents exhibited flake-like structures formed due to the aggregation of the several thousands of nanoparticles. The flakes are dense and interconnected with each other, such that no clear boundaries exist between one another. However, MgO nanoflakes obtained using EDA (Fig. 3d) as solvent appear to be stacked to build up coral-like hierarchical structures. Such kinds of coral-like structures are beneficial for catalysis, since the voids between adjacent nanoflakes allow the efficient transport of reactant molecules to the active sites, and enhance the reaction/interaction between the photocatalyst and the interacting molecules.

3.3. Optical studies

Fig. 4(a) shows the typical UV DRS of MgO nanocrystals prepared using different solvents. The absorption onset was calculated by the extrapolation method, i.e., extrapolating the tangent of the steep absorption curve to intercept the wavelength axis. The energy band gap of MgO nanocrystals was found using [28,29]

$$E_g(eV) = \frac{1240}{\lambda_g} \tag{4}$$

where 'λ_g' is the wavelength of the intercept. The optical band gaps of MgO nanocrystals prepared using different solvents are given in Table 1 and the calculated values are in good agreement with earlier reports [30,31].

Fig. 4(b) shows the PL spectra of MgO nanocrystals synthesized using different solvents. Although MgO is a typical wide band gap insulator, the PL properties of MgO nanocrystals have been studied because of the presence of

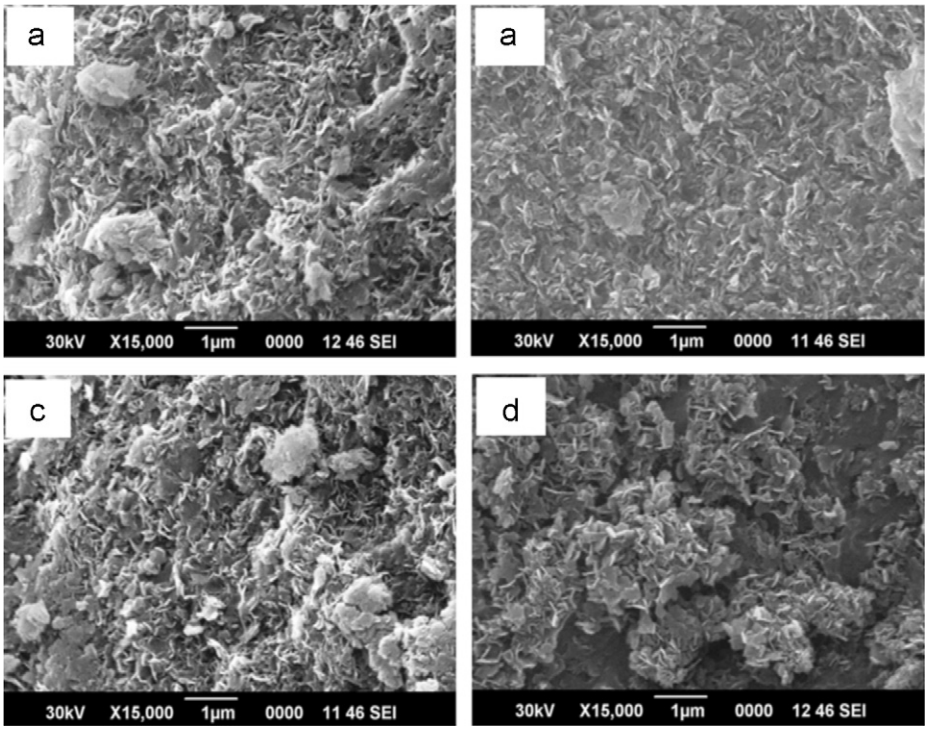

Fig. 3. SEM images of (a) sample *A*, (b) sample *B*, (c) sample *C*, and (d) sample *D*.

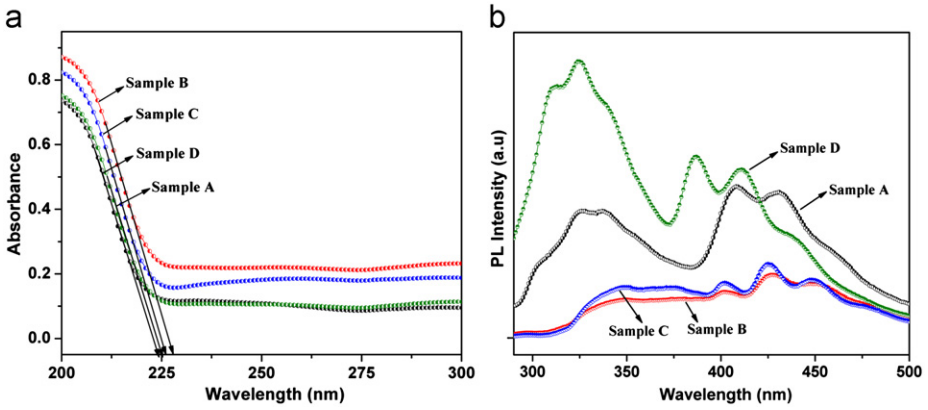

Fig. 4. (a) UV DRS, and (b) PL spectra of MgO nanoflakes prepared using different solvents.

defects [31]. The position of the emission peaks of MgO nanocrystals synthesized using different solvents remains unaltered, whereas the relative intensities of the peaks differ. Clearly, the PL bands are not due to band gap emissions, but can be attributed to various structural defects. The rapid evaporation and incomplete crystallization may generate various structural defects, contributing to the observed emissions in MgO nanocrystals [24]. MgO nanocrystals synthesized using HMTA and TEA as solvents exhibit a violet emission peak at 401 nm, while the MgO nanocrystals synthesized using EDA and water as solvents exhibit violet emission peaks at 386 nm and 408 nm respectively. The blue emission peaks were observed at 425 nm and 448 nm when TEA and HMTA were respectively used as solvents. In the case of EDA, blue emission peaks were observed at 412 nm and 438 nm, whereas for water the blue emission peaks were observed at 431 nm and 460 nm. Generally, the violet emission peaks are attributed to the oxygen ion vacancies in the bulk of MgO, while the blue peaks are ascribed to the structural defects such as Mg vacancies and interstitials [32–34]. The change in the peak intensity and peak positions of MgO nanocrystals indicates the changes in the concentration of defects, since the formation conditions, morphology and size of the crystallites may alter the density of defects and surface states [13,35].

3.4. Photocatalytic activity of MgO

Azo dyes which constitute a major part of all commercial dyes are toxic, mutagenic and carcinogenic [36]. Fifty to sixty percent of the dyes used in the textile industries are azo dyes containing one or more azo bonds (–N N–) [36,37]. MO ($C_{14}H_{14}N_3.SO_3Na$) is one of the representative azo classes of dyes, the most important class of synthetic organic dyes used in the textile industry, and also a common industrial pollutant [38]. Since the band gap of MgO is much larger than the energy of UV illumination, the generation of reactive species like OH radicals takes place due to the native defects [18]. The photocatalytic activities of the synthesized MgO nanoflakes were evaluated by monitoring the degradation in MO solution.

Fig. 5 shows the typical time-dependent UV–vis absorption spectra of MO solution after UV irradiation with MgO nanocrystals (sample D) as photocatalyst obtained using EDA as solvent. The characteristic absorption of MO at 465 nm decreased rapidly with extension of the irradiation time, and completely disappeared after 90 min of irradiation. The decrease in the characteristic absorption of MO indicates the degradation of polyaromatic rings in methyl orange to monosubstituted aromatics, and the disappearance of the MO absorption band at $t=90$ min suggests that the functional group responsible for the characteristic color of MO dye is broken down. Similarly, samples *A–C* degrade MO in 120 min. It was observed that MO solution turns totally colorless after irradiation for different time durations, indicating the complete decomposition of MO molecules by MgO nanocrystals. Variation of MO dye solution during the photodegradation process was examined using HPLC and is shown in Fig. 6. The HPLC analysis of pure MO dye sample (Fig. 6(a)) before treatment showed a major peak at 3.3 mins retention time. With addition of MgO catalyst (Figs. 6(b) and 6(c)), the intensity of the major peaks decreases, indicating degradation of MO dye. The intensities of the other peaks at higher retention times increased at first and subsequently decreased, indicating the formation and transformation of the intermediates.

Fig. 7 shows the comparison of degradation efficiency of MgO nanoflakes prepared using different solvents. Although all samples could bleach the MO solution, different photocatalytic activities were observed among them. The MgO

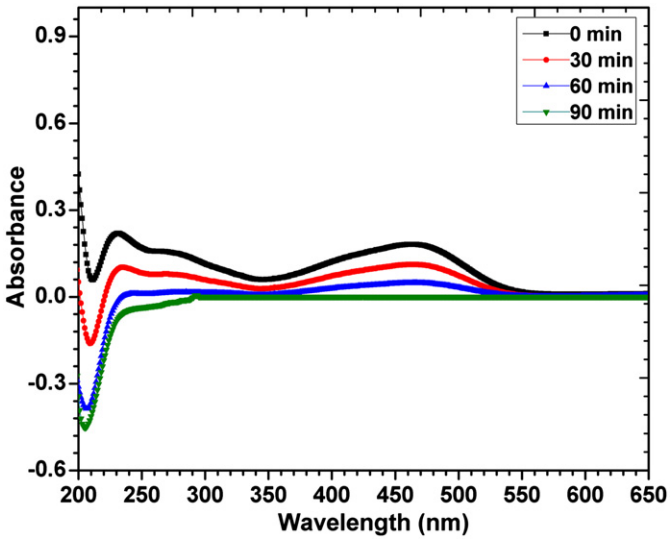

Fig. 5. Time-dependent UV–vis absorption spectra of MO solution after UV-light irradiation with MgO nanoflakes (sample *D*).

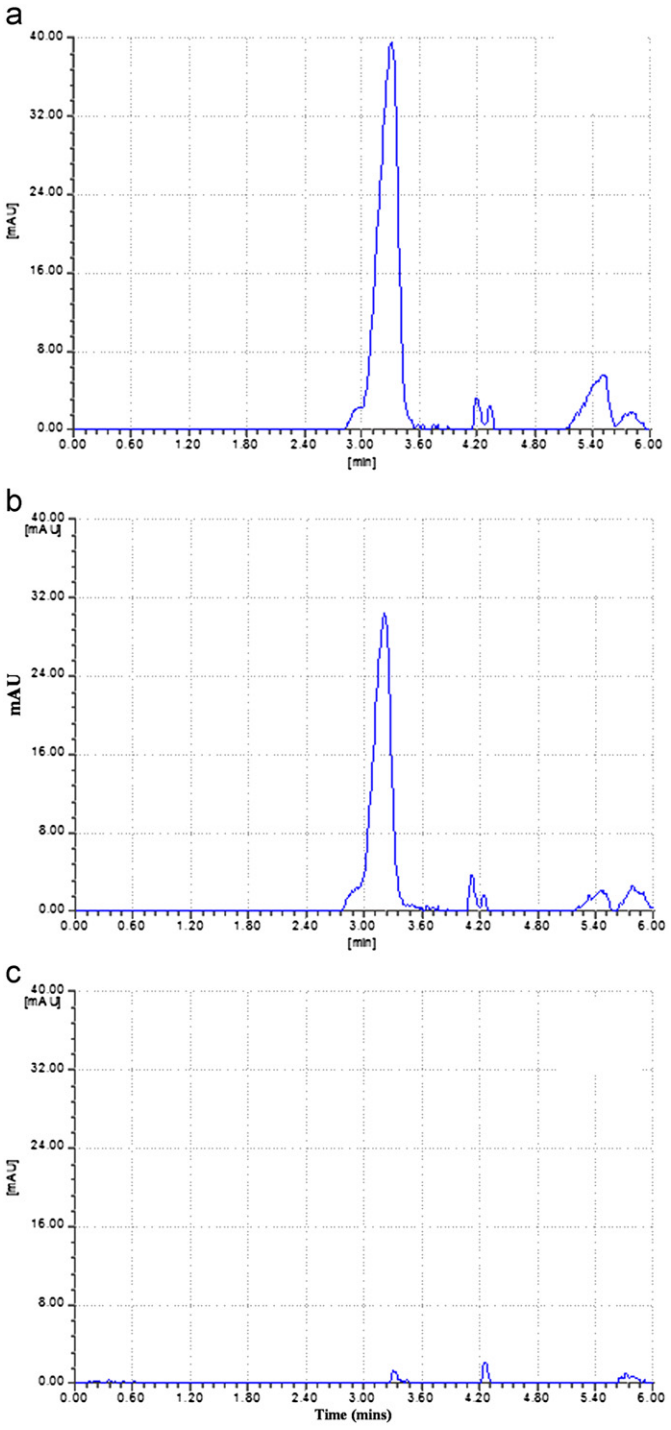

Fig. 6. HPLC of (a) pure MO dye, and at different times during degradation:(b) 0 min, and (c) 90 min.

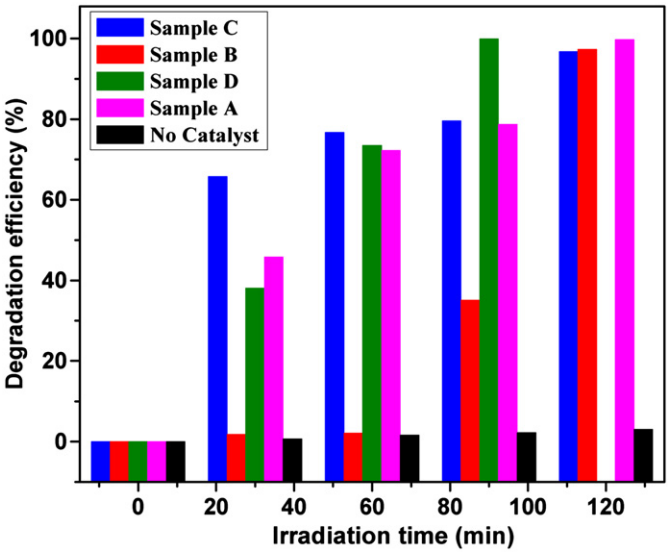

Fig. 7. MO degradation efficiency of MgO nanoflakes synthesized using different solvents.

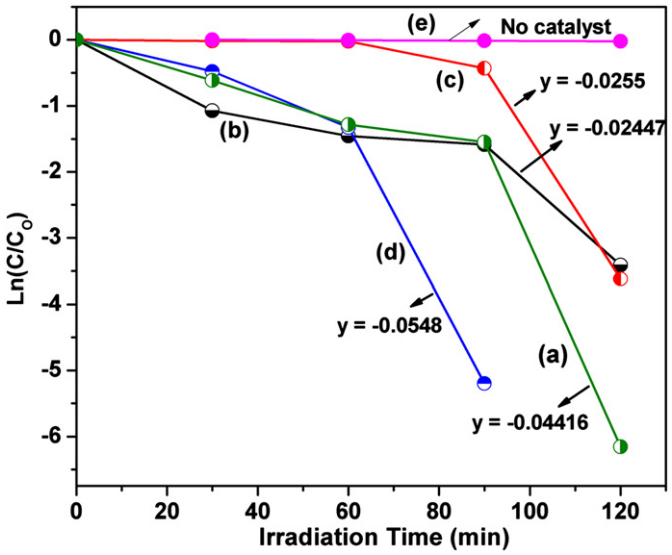

Fig. 8. Degradation kinetics of MO using MgO nanoflakes as photocatalyst:(a) sample *A*, (b) sample *B*, (c) sample *C*, (d) sample *D*, and (e) without catalyst.

nanoflakes prepared using different solvents have the same photocatalytic efficiency ($\eta=0$) in the dark ($t=0$), which dictates that photocatalytic reaction is induced with the aid of UV light irradiation. The degradation efficiency in the absence of MgO catalyst was found to be 3% at $t=250$ min. The photodegradation efficiency of samples *A*, *B,* and, *C* were found to be 99.79%, 97.32%, and 96.70% respectively at $t=120$ min, while that of sample D was found to be 99.94% at $t=90$ min. Though the real mechanism for photocatalytic activity of MgO is debatable, the generation of OH radicals due to native defects is likely to be responsible for the photocatalytic activity in MgO. Since the band gap of MgO is very large, the intrinsic band gap excitation of MgO for photoreaction is not possible, and hence the generation of OH radicals due to native defects induces photodegradation. As seen from FTIR, there is an adsorption of several carbonate species (unidentate, bidentate, and bicarbonate) on the surface of MgO, and the adsorbed carbonate ions introduce new defect levels. Hence, photodegradation occurs due to the direct electron transfer from a new defect level generated between the HOMO (the valence band) and LUMO (the conduction band) levels of MgO by the formation of a surface complex (bidentate carbonate–MgO) to LUMO or from HOMO to a new defects level.

The degradation kinetic curves of MO using MgO nanoflakes as the photocatalyst is shown in Fig. 8. The degradation kinetics was studied by plotting the natural logarithm of concentration ratio, $\ln(C/C_o)$, versus the irradiation time, t. It can be seen that the concentration ratio in ln scale changes linearly with time, indicating that the photodegradation of MO follows the first-order kinetics. The kinetic parameters such as degradation efficiency, degradation rate constant (K_r), half life values ($t_{1/2}$) and linear co-efficient (R^2) are calculated from the kinetics plot, and are given in Table 2. The high degradation efficiency and rate constant of MgO nanoflakes synthesized using EDA as a solvent indicates the superior photocatalytic activity.

The high photocatalytic activity of MgO nanocrystals synthesized using EDA as solvent can be attributed to the smaller crystallite size and high number of defects as evident from XRD and PL spectra respectively. Due to smaller crystallite size the number of atoms with unsaturated coordination on the surface is large, and these chemically more active atoms play a major role in enhancing the photocatalytic reaction. Also, the presence of a large number of defect sites makes catalysts to have high chemical activities. The photogenerated electrons and holes in these defect energy levels can act as the active sites for photocatalytic reaction because they can also be trapped by oxygen and surface hydroxyl species [39,40]. Also, when a suitable scavenger or surface defect site is available to trap the electron or hole, recombination is prevented and subsequent redox reactions occur. In addition, the photocatalytic performance was also influenced by various factors, such as crystallite size, specific surface area, morphology and texture [41]. As seen from SEM analysis, the voids among the nanoflakes of the coral-like MgO structure (sample *D*) allow efficient transport of reactant molecules to get to the active sites, thereby enhancing the reaction/interaction between the photocatalyst and the interacting molecules, and improving the photocatalytic efficiency. These experimental results demonstrate that MgO can be used as a prospective candidate for photodegradation of organic pollutants.

4. Conclusion

MgO nanoflakes were synthesized by a facile route based on the thermal decomposition of the precursor obtained

Table 2
Kinetic parameters for photocatalytic degradation of MO solution.

Sample code	Absorption		Degradation (%)	K_r (min^{-1})	$t_{1/2}$ (min)	R^2
	Before irradiation	After irradiation				
A	1.888	0.004	99.79	0.0442	15.70	0.6461
B	0.336	0.009	97.32	0.0255	27.18	0.4523
C	0.485	0.016	96.70	0.0245	28.33	0.8449
D	0.181	0.0001	99.94	0.0548	12.65	0.7109

from reflux condensation approach prepared using different solvents. XRD and FTIR confirmed the formation of single phase MgO with cubic structure. SEM images exhibited flake-like morphology. PL measurements showed defect emissions in the visible region arising due to various structural defects like Mg interstitials and O vacancies. MgO nanoflakes synthesized using different solvents showed good photocatalytic activity towards the MO dye. MgO nanoparticles synthesized using different solvents exhibited different levels of photodegradation due to the variation in crystallite size, defect concentrations, and morphology. In particular, MgO nanoflakes synthesized using EDA as solvent exhibited good photocatalytic activity due to the coral-like structure and presence of a large number of defects. Finally, it can be anticipated that our results will explore the viability of using MgO as a prospective candidate for degrading organic pollutants.

References

[1] U.I. Gaya, A.H. Abdullah, Z. Zainal, M.Z. Hussein, Photocatalytic treatment of 4-chlorophenol in aqueous ZnO suspensions: intermediates, influence of dosage and inorganic anions, Journal of Hazardous Materials 168 (2009) 57–63.

[2] M.C. Yeber, J. Rodriguez, J. Freer, N. Durán, H.D. Mansilla, Photocatalytic degradation of cellulose bleaching effluent by supported TiO_2 and ZnO, Chemosphere 41 (2000) 1193–1197.

[3] S. Chakrabarti, B.K. Dutta, Photocatalytic degradation of model textile dyes in wastewater using ZnO as semiconductor catalyst, Journal of Hazardous Materials 112 (2004) 269–278.

[4] M.A. Behnajady, S.G. Moghaddam, N. Modirshahla, M. Shokri, Investigation of the effect of heat attachment method parameters at photocatalytic activity of immobilized ZnO nanoparticles on glass plate, Desalination 249 (2009) 1371–1376.

[5] M.A. Mahmood, S. Baruah, J. Dutta, Enhanced visible light photocatalysis by manganese doping or rapid crystallization with ZnO nanoparticles, Materials Chemistry and Physics 130 (2011) 531–535.

[6] G.K. Prasad, P.V.R.K. Ramacharyulu, Beer Singh, K. Batra, Anchal R. Srivastava, K. Ganesan, R. Vijayaraghavan, Sun light assisted photocatalytic decontamination of sulfur mustard using ZnO nanoparticles, Journal of Molecular Catalysis A: Chemical 349 (2011) 55–62.

[7] X. Jiang, L. Yang, P. Liu, X. Li, J. Shen, The photocatalytic and antibacterial activities of neodymium and iodine doped TiO_2 nanoparticles, Colloids and Surfaces B: Biointerfaces 79 (2010) 69–74.

[8] E. Yassıtepe, H.C. Yatmaz, C. Ozturk, K. Ozturk, C. Duran, Photocatalytic efficiency of ZnO plates in degradation of azo dye solutions, Journal of Photochemistry and Photobiology A 198 (2008) 1–6.

[9] A.M. Cruz, D.S. Martinez, E.L. Cuellar, Synthesis and characterization of WO_3 nanoparticles prepared by the precipitation method: evaluation of photocatalytic activity under vis-irradiation, Solid State Sciences 12 (2010) 88–94.

[10] J. Gu, S. Li, E. Wang, Q. Li, G. Sun, R. Xu, H. Zhang, Single-crystalline α-Fe_2O_3 with hierarchical structures: controllable synthesis, formation mechanism and photocatalytic properties, Journal of Solid State Chemistry 182 (2009) 1265–1272.

[11] J. Li, F. Sun, K. Gu, T. Wu, W. Zhai, W. Li, S. Huang, Preparation of spindly CuO micro-particles for photodegradation of dye pollutants under a halogen tungsten lamp, Applied Catalysis A: General 406 (2011) 51–58.

[12] G. Duan, X. Yang, J. Chen, G. Huang, L. Lu, X. Wang, The catalytic effect of nanosized MgO on the decomposition of ammonium perchlorate, Powder Technology 172 (2007) 27–29.

[13] H. Niu, Q. Yang, K. Tang, Y. Xie, Self-assembly of porous MgO nanoparticles into coral-like microcrystals, Scripta Materialia 54 (2006) 1791–1796.

[14] M.A. Shah, A. Qurashi, Novel surfactant-free synthesis of MgO nanoflakes, Journal of Alloys and Compounds 482 (2009) 548–551.

[15] W. Wang, X. Qiao, J. Chen, F. Tan, H. Li, Influence of titanium doping on the structure and morphology of MgO prepared by coprecipitation method, Materials Characterization 60 (2009) 858–862.

[16] T. Qiu, X.L. Wu, F.Y. Jin, A.P. Huang, P.K. Chu, Self-assembled growth of MgO nanosheet arrays via a micro-arc oxidation technique, Applied Surface Science 253 (2007) 3987–3990.

[17] M. Anpo, Y. Yamada, Photoluminescence and photocatalytic activity of MgO powders, Materials Chemistry and Physics 18 (1988) 465–484.

[18] M.Y. Guo, A.M. Ching, Ng F. Liu, A.B. Djurisic, W.K. Chan, Photocatalytic activity of metal oxides—the role of holes and OH radicals, Applied Catalysis B: Environmental 107 (2011) 150–157.

[19] J. Tian, J. Wang, J. Dai, X. Wang, Y. Yin, N-doped TiO_2/ZnO composite powder and its photocatalytic performance for degradation of methyl orange, Surface and Coatings Technology 204 (2009) 723–730.

[20] J. Wang, X.M. Fan, Z.W. Zhou, K. Tian, Preparation of Ag nanoparticles coated tetrapod-like ZnO whisker photocatalysts using photoreduction, Materials Science and Engineering: B 176 (2011) 978–983.

[21] Y. Zhang, J. Mu, One-pot synthesis, photoluminescence, and photocatalysis of Ag/ZnO composites, Journal of Colloid and Interface Science 309 (2007) 478–484.

[22] X. Li, Y. Cheng, S. Kang, J. Mu, Preparation and enhanced visible light-driven catalytic activity of ZnO microrods sensitized by porphyrin heteroaggregate, Applied Surface Science 256 (2010) 6705–6709.

[23] M. Rezaei, M. Khajenoori, B. Nematollahi, Preparation of nanocrystalline MgO by surfactant assisted precipitation method, Materials Research Bulletin 46 (2011) 1632–1633.

[24] N. Clament Sagaya Selvam, R. Thinesh Kumar, L. John Kennedy, J. Judith Vijaya, Comparative study of microwave and conventional methods for the preparation and optical properties of novel MgO-micro and nano-structures, Journal of Alloys and Compounds 509 (2011) 9809–9815.

[25] J. Zhou, S. Yang, J. Yu, Facile fabrication of mesoporous MgO microspheres and their enhanced adsorption performance for phosphate from aqueous solutions, Colloids and Surfaces A: Physicochemical and Engineering Aspects 379 (2011) 102–108.
[26] Z. Zhao, H. Dai, Y. Du, J. Deng, L. Zhang, F. Shi, Solvo- or hydrothermal fabrication and excellent carbon dioxide adsorption behaviors of magnesium oxides with multiple morphologies and porous structures, Materials Chemistry and Physics 128 (2011) 348–356.
[27] H. Niu, Q. Yang, K. Tang, Y. Xie, Large-scale synthesis of single-crystalline MgO with bone-like nanostructures, Journal of Nanoparticle Research 8 (2006) 881–888.
[28] L. Ren, Y.P. Zeng, D. Jiang, The improved photocatalytic properties of p-type NiO loaded porous TiO_2 sheets prepared via freeze tape-casting, Solid State Sciences 12 (2010) 138–143.
[29] G.Q. Zhang, N. Chang, D.Q. Han, A.Q. Zhou, X.H. Xu, The enhanced visible light photocatalytic activity of nanosheet-like Bi_2WO_6 obtained by acid treatment for the degradation of rhodamine B, Materials Letters 64 (2010) 2135–2137.
[30] L. Kumari, W.Z. Li, C.H. Vannoy, R.M. Leblanc, D.Z. Wang, Synthesis, characterization and optical properties of $Mg(OH)_2$ micro–/nanostructure and its conversion to MgO, Ceramics International 35 (2009) 3355–3364.
[31] F. Mohandes, F. Davar, M. Salavati-Niasari, Magnesium oxide nanocrystals via thermal decomposition of magnesium oxalate, Journal of Physics and Chemistry of Solids 71 (2010) 1623–1628.
[32] H.W. Kim, S.H. Shim, Growth of MgO nanowires assisted by the annealing treatment of Au-coated substrates, Chemical Physics Letters 422 (2006) 165–169.
[33] H.W. Kim, S.H. Shim, J.W. Lee, M.A. Kebede, H.H. Yang, M.H. Kong, S.M. Choi, J.H. Yang, H.J. Bang, H.Y. Kim, Coating of MgO nanorods with protective layers: sputtering with a Si target, structure, and photoluminescence properties, Surface and Coatings Technology 202 (2008) 2503–2508.
[34] F.L. Deepak, P. Saldanha, S.R.C. Vivekchand, A. Govindaraj, A study of the dispersions of metal oxide nanowires in polar solvents, Chemical Physics Letters 417 (2006) 535–539.
[35] N. Kumar, D. Sanyal, A. Sundaresan, Defect induced ferromagnetism in MgO nanoparticles studied by optical and positron annihilation spectroscopy, Chemical Physics Letters 477 (2009) 360–364.
[36] A. Behnajady, N. Modirshahla, N. Daneshvar, M. Rabbani, Photocatalytic degradation of C.I. Acid Red 27 by immobilized ZnO on glass plates in continuous-mode, Journal of Hazardous Materials 140 (2007) 257–263.
[37] N. Kaneva, I. Stambolova, V. Blaskov, Y. Dimitriev, A. Bojinova, C. Dushkin, A comparative study on the photocatalytic efficiency of ZnO thin films prepared by spray pyrolysis and sol–gel method, Surface and Coatings Technology. (2011) In press.
[38] Y. Zhang, F. Zhu, J. Zhang, L. Xia, Converting layered zinc acetate nanobelts to one-dimensional structured ZnO nanoparticle aggregates and their photocatalytic activity, Nanoscale Research Letters 3 (2008) 201–204.
[39] Y. Li, X.Y. Yang, J. Rooke, G. Van Tendeloo, B.L. Su, Ultralong $Cu(OH)_2$ and CuO nanowire bundles: PEG200-directed crystal growth for enhanced photocatalytic performance, Journal of Colloid and Interface Science 348 (2010) 303–312.
[40] Y. Lai, M. Meng, Y. Yu, X. Wang, T. Ding, Photoluminescence and photocatalysis of the flower-like nano-ZnO photocatalysts prepared by a facile hydrothermal method with or without ultrasonic assistance, Applied Catalysis B: Environmental 105 (2011) 335–345.
[41] A. Umar, M.S. Chauhan, S. Chauhan, R. Kumar, G. Kumar, S.A. Al-Sayari, S.W. Hwang, A. Al-Hajry, Large-scale synthesis of ZnO balls made of fluffy thin nanosheets by simple solution process: Structural, optical and photocatalytic properties, Journal of Colloid and Interface Science 363 (2011) 521–528.